SECRETARIA DE PLANEJAMENTO DA PRESIDÊNCIA DA REPÚBLICA

CONSELHO NACIONAL DE DESENVOLVIMENTO CIENTÍFICO E TECNOLÓGICO

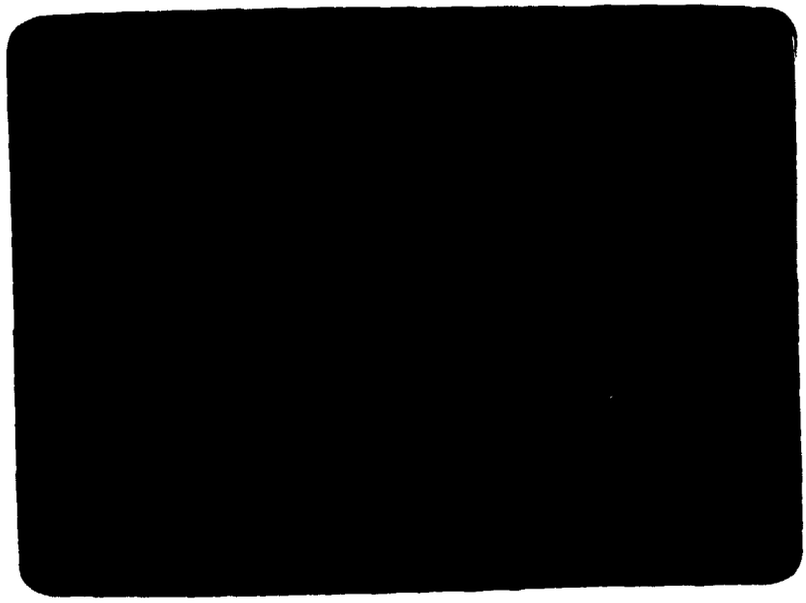

INSTITUTO DE PESQUISAS ESPACIAIS

1. Publication NO	2. Version	3. Date	5. Distribution
INPE-2260-PRE/042	3rd	Nov., 1981	☐ Internal ☒ External ☐ Restricted
4. Origin: DGA/DII	Program: ELIS		

6. Key words - selected by the author(s)
IONOSPHERE
NIGHTGLOW
EQUATORIAL PLASMA BUBLES

7. U.D.C.: 523.4-853

8. Title: INPE-2260-PRE/042

A SIMULATION OF EQUATORIAL PLASMA BUBBLE SIGNATURES ON THE OI 6300 Å NIGHTGLOW MERIDIONAL PROFILE OVER BRAZILIAN LOW LATITUDE

10. NO of pages: 44

11. Last page: 41

12. Revised by

J. A. Bittencourt

9. Authorship: Y. Nakamura
J.H.A. Sobral
M.A. Abdu

14/10

13. Authorized by

Nelson de Jesus Parada
Director

Responsible author

14. Abstract/Notes: The [OI] 6300 Å nightglow emission measurements carried out by scanning photometers over Cachoeira Paulista (geogr. coord. 22°41'S, 45°W, geom. coord. 11°57'S, 22°32'E) often show propagating disturbances on the meridional and east-west intensity profiles. The disturbances propagate from north to south and from west to east. Extensive measurements of these disturbances have been carried out at Cachoeira Paulista, and the results have shown that they are closely correlated with the occurrence of spread F irregularities observed by ionosonde. A quantitative interpretation of the meridional propagation of the airglow disturbance is attempted by carrying out a numerical simulation of the phenomenon. Airglow intensity as a function of zenith angle in the photometer scanning range was calculated using electron density profiles perturbed by field aligned plasma bubble, whose vertical velocity and electron density depletion profile were determined from a numerical simulation of the nonlinear Rayleigh-Taylor instability under ionospheric conditions that best represented those of the observing period and location. The result of the simulation shows clearly that, as the field aligned plasma bubbles rises up over the equator, their extremities trace out poleward motion in the low latitude ionosphere which could explain the observed north to south propagation of the airglow intensity valleys.

15. Remarks

This work will be submitted to Annales Geophysicae.
Revised in April 1983.

A SIMULATION OF EQUATORIAL PLASMA BUBBLE SIGNATURES ON THE OI 6300 Å NIGHTGLOW MERIDIONAL PROFILE OVER BRAZILIAN LOW LATITUDE

Y. Nakamura, J.H.A. Sobral, and M.A. Abdu

Instituto de Pesquisas Espaciais - INPE
Conselho Nacional de Desenvolvimento Científico e Tecnológico - CNPq
12200 - São José dos Campos, SP, Brasil

ABSTRACT

The [OI] 6300 Å nightglow emission measurements carried out by scanning photometers over Cachoeira Paulista (geogr. coord. 22°S, 45°W, geom. coord. 11°57'S, 22°32'E) often show propagating disturbances on the meridional and east-west intensity profiles. The disturbances propagate from north to south and from west to east. Extensive observations of these disturbances have been carried out at Cachoeira Paulista, where strong correlation has been observed between these events and the range type spread F occurrences, thus identifying them as the airglow manifestations of the equatorial plasma bubble (or depletion) events. The low latitude footprints of the field aligned plasma depletions could have two types of characteristic signatures in the scanning photometer data: (a) events that have their onsets well westward of the photometer observing longitude, representing the post growth phase of a bubble event; such events could cause an apparent meridional propagation of the airglow valleys in the north-south scan data. On the other hand (b) those events having onsets in the vicinity of the photometer longitude could be representing the growth phase of a bubble event and, therefore, the north-south scan could detect meridional propagation of the airglow valleys caused by vertical rise of the head region of plasma bubble over the magnetic equator. In both cases (a) and (b) the east-west scan photometer detects the eastward propagation of the plasma depletions. In this paper a quantitative interpretation of the meridional propagation of the airglow disturbance

for the type (b) events is attempted by carrying out a numerical simulation of the phenomenon. Airglow intensity as a function of zenith angle in the photometer scanning range was calculated using electron density profiles perturbed by field aligned plasma bubble, whose vertical velocity and electron density depletion profile were determined from a numerical simulation of the nonlinear Rayleigh-Taylor instability under ionospheric conditions that best represented those of the observing period and location. The result of the simulation shows clearly that, as the field aligned plasma bubbles rises up over the equator in their growth phases, their extremities trace out poleward motion in the low latitude ionosphere which could explain the observed north to south propagation of the airglow intensity valleys, observed in the early post sunset hours.

INTRODUCTION

Regular measurements of meridional and east-west profiles of night airglow intensity in the [OI] 6300 Å emission line has been carried out at Cachoeira Paulista, (22^{o}S, 45^{o}W) Brazil, a low latitude station, for the past few years. The scanning photometers used for the observations cover 75^{o} in both the meridional and the east-west planes. The relevant details of the instrumentation have been described by Sobral et al. (1980a). Preliminary analysis of the observational data has revealed the presence of propagating disturbances in the airglow intensity profiles occurring as a regular feature, depending upon the season, in the ionosphere over Cachoeira Paulista, some characteristics of which have already been published by Sobral et al. (1980a, b, 1981; see, also, Sahai et al., 1981). These nightglow disturbances (ND's) usually occur during premidnight hours in summer and equinoctial months, and propagate predominantly away from the equator. Further, almost hundred percent correlation was observed between their occurrence and that of the range type spread F in the ionograms over Cachoeira Paulista (Sobral et al., 1980b), thus indentifying these disturbances as airglow manifestation of the spread F irregularity dynamics. VHF radar investigations by Woodman and La Hoz (1976) and by Tsunoda (1980) and satellite ion density measurements by McClure et al., (1977) have shown that the spread F irregularities occur in plasma depleted regions (Hanson and Sanatani, 1973), widely known as plasma bubbles, in the equatorial ionosphere. The irregularity and the background plasma density distribution as mapped by the ALTAIR steerable vhf radar by Tsunoda (1980) show that the plasma bubbles and associated irregularities occur strongly field aligned extending hundreds of kilometers into the low latitude ionosphere on either side of the equator (see also Aarons et al., 1980; Dyson and Benson, 1978; Dachev and Walker, 1982). Low latitude observations of north-south elongated airglow depletion patches by Weber et al. (1980) (see also Mendillo and Baumgardner 1982) have corroborated these characteristics of the plasma bubbles.

The primary processes that are responsible for the generation of the plasma bubble are believed to be the wellknown Rayleigh-Taylor (R-T) fluid instability mechanism originally suggested by Dungey (1956), and under some circumstances also the gradient drift instability (see Reid, 1968). Theoretical investigation of plasma bubble by the R-T mechanism has been carried out by several authors (Haerendel, 1973; Chaturvedi and Kaw, 1975; Hudson and Kennel, 1975; Ott, 1978) and experimental evidence to this effect has been suggested from rocket and radar observations carried out over Natal, Brazil (Kelley et al., 1976, also Woodman and La Hoz 1976). Numerical simulation of the bubble dynamics under the conditions of collisional R-T regime has been carried out by Scannapieco and Ossakow (1976) and Ossakow et al., (1979) using local ionospheric model (see also Anderson and Haerendel 1979) strong correlation has been found by Abdu et al. (1982) between the collisional R-T instability growth rate conditions and the occurrences of range type spread F in the ionograms over the magnetic equatorial station Fortaleza.

In the papers by Sobral et al., (1980a, b, 1981) it was suggested that the vertical rise of the plasma bubble, in the equatorial ionosphere would trace out poleward extension of the bubble (see also Weber et al., 1980). Such possibility of a "footprint" in the low latitude ionosphere of rising equatorial plasma bubble were also suggested earlier from AE-C measurements of plasma depletions by McClure et al. (1977). The resulting poleward propagation of extremities of the plasma bubble was suggested as an explanation for the propagation of the airglow depletion valleys, away from the equator, observed in the meridional scanning photometer data. The key point in the interpretation of the meridional photometer scanning data is the magnetic flux tube alignment characteristics of the plasma bubble. The interpretation of Sobral et al. was, however, based on somewhat qualitative premises. In this paper we discuss further characteristics of the airglow disturbances and attempt to provide a quantitative basis to the interpretation given by Sobral et al..This will be done based on a detailed comparison of the different characteristics of the ND's

observed in the scanning data with the wellknown dynamic features of the plasma bubble observed from vhf radars, satellites and airglow imaging techniques reported by other researchers.

CHARACTERISTICS OF THE AIRGLOW DISTURBANCES

The scanning data that would represent a quiet ionosphere condition (namely, horizontally stratified condition) would be like an extended "U" curve. In the meridional scanning data in the post sunset hours the airglow intensity would, sometimes, be stronger in either northern or in southern half of the scanning range depending upon the location of the intertropical red arc, the airglow signature of the Appleton anomaly crest, (Sobral et al., 1980a), that usually passes over Cachoeira Paulista at post sunset hours during the equinoctial months. An airglow meridional profile representative of such "quiet" condition would be somewhat similar to the curve at 2128 LT in Figure 1a (when the small scale fluctuation at the southern end and the small kink at the northern end are ignored). The minor kinks at the northern edge present in the curves at 2123 and 2128 LT seem to have developed into the airglow valley seen very pronounced in the curve at 2139 LT. The size of the valley on this curve can be judged by comparing the solid line, the measured airglow intensity, with the dashed curve drawn to represent the undisturbed curve at 2139LT. The propagation, southward, of this valley is seen accompanied by the propagation of a corresponding valley from west to east in the east-west scanning photometer data presented in the part(b) of the same figure. The amplitude of the valley in the E-W scanning data may be judged with respect to the dashed line drawn to represent the unperturbed intensity curve at 2139 LT.

Majority of these post sunset nightglow disturbances (denoted as ND's) had their onset in the N-S scan data around 2100 LT. In an arbitrary sample of 19 events considered the earliest occurrence was observed at 1953 LT and the latest was at 2231LT. As reported earlier by Sobral et al. (1980b) all the ND's were associated with

range type spread F events in the ionograms over Cachoeira Paulista, the onsets of which were usually somewhat earlier than the onsets of the ND's. The delay in the ND onsets varied from 6 minutes up to 75 minutes (some of the cases of large delay are likely to be caused by the difficulty in identifying the onsets of very weak ND's). The mean time delay of the data considered was ~35 minutes, which could easily be accounted for by the ability of the ionosonde to receive spread F echoes from oblique directions. In fact, the ionosonde is capable of detecting irregularity structures ~10 minutes ahead or behind the local time and the passage over local meridian of such irregularities at, say, 100 m s^{-1} could involve a time delay of the order of 45 minutes.

The onset times of the valleys in Figure (1) seem to be slightly earlier in the N-S scan than in the E-W scan. The widths of the airglow valleys in the E-W scan should, in fact, represent a corresponding width for the plasma bubble in the equatorial plane. The average east-west dimension of the valleys is estimated as 315 km with a standard deviation of 52 km. The eastward velocity is estimated as 220 m s^{-1}. In the N-S scanning data the width of the first set of valleys is found to vary from 909 to 688 km, generally decreasing southward, the mean width being 766 ± 72 km. When the valley that started at about 2133 LT reached the near end of the scanning range of the respective photometers, a second valley appears in the northwest and follows the same direction as the first one. The propagation velocities, typical for these disturbances, as mean values during a given passage, have been presented earlier by Sobral et al., (1980a). For this specific event the southward velocity is estimated as -300 m s^{-1}. An analysis of a number of events registered by the north-south scanning photometer is presented below in order to see if the velocities of the individual valleys remain constant throughout the scanning range of the photometer.

Figure 2 shows the positions of the valleys in horizontal distances, with reference to the zenith position, as a function of

time for 18 events of ND's. For a given event in this figure the zero time was attributed to the valley minimum at the midpoint of the scanning range (zenith), resulting in positive times for the valleys on the southern half and negative time for the valleys on the northern half of the scanning range. The position of the valley was read during each scanning, namely, at an interval of approximately 4.5 minutes. The points from the resulting scatter plot was then used to determine the mean distance of the valley during time intervals of 200 seconds. These distances are marked (x) at the middle of the time interval, and a second order polinomial fit of these points drawn by the solid line clearly indicate that the north-south velocity component of the valley decreases from north to south. In general, the velocities in the northern half are higher than in the southern half of the scanning range. This point has important implications as will be discussed later.

Of the 18 cases of the ND's analysed above, seven of the events were present either on the northern half or on the southern half of the scanning range. 11 cases presented the disturbances throughout the scanning range. For these cases, the southward velocities were calculated at north and at south separately using least square fitting and assuming emission height of 300 km. Table 1 shows the velocities at north and at south for the individual cases. The mean velocity to the north comes out to be 305 ± 159 m/s, the velocity to the south being 246 ± 105 m/s.

A statistical analysis of the amplitude variations of these disturbances with zenith angle was carried out for 14 nights and the result is presented in Figure 3. The least square fit line shows a tendency for the amplitude to decrease from north towards south. This may be explained by the fact that when the photometer looks north (south), it sees the bubble approximately along (across) the geomagnetic field line, which result in larger (smaller) airglow perturbation amplitudes.

RELATIONSHIP BETWEEN THE PLASMA BUBBLE DYNAMICS AND ND VELOCITIES

The east-west displacement of the airglow valleys could, in a rather straightforward way, represent an east-west velocity of the plasma bubble in the equatorial plane due to the large north-south extension of the plasma bubble. In fact, the eastward velocities determined from Figure 1, as 100-150 m s^{-1}, compares well with the eastward drift velocities of irregularity plumes observed by Tsunoda (1981) and Woodman and La Hoz (1976), with the plasma bubble velocities measured from satellite by McClure et al. (1977) and with the scintillation patch velocities discussed by Basu and Kelley (1979). On the other hand the interpretation of the poleward displacement of the airglow valleys in the meridional scan data would involve also detailed considerations on the shape,and orientation, transverse to the magnetic field, of the plasma bubble.

Extensive measurements of these and other important dynamical features of the equatorial plasma bubble have been carried out with the ALTAIR steerable radar (see for example, Tsunoda, 1981; Tsunoda et al., 1981, 1982). In particular, Tsunoda et al. (1982) has addressed the question of two-dimensional shape of the plasma bubble transverse to the geomagnetic field, by comparing the east-west spatial relationship of ion density depletion measured in-situ by the Atmospheric Explorer-E (AE - E) satellite with backscatter plumes measured by the ALTAIR radar. Their results show, in agreement with the results from theoretical modelling (Ossakow et al., 1979; Zalesak and Ossakow 1980) that plasma bubbles are vertically elongated depletions that extend from the bottomside of the F-layer, having a well defined neck region (namely, a vertical channel or wedge) that is significantly narrower than, but probably equally depleted of the ionization as, the head region. They develop with the head region tilted westward of the vertical by as much as ~40^0 as some of the plume maps of Tsunoda (1981) and Tsunoda et al., (1982) indicate. Evidence for such tilts was seen also in the airglow photographs taken by Weber et al. (1980) (see also Moore and Weber, 1981; Mendillo and

Baumgardner, 1982) that showed westward tilts, with respect to the magnetic meridian, of elongated 6300 Å depletion patches produced as low latitude footprint of the plasma bubble. Tsunoda (1981) showed that the typical growth phase of a plasma bubble (or plume) event lasts of the order of 50 minutes during which the vertical rise velocity of the bubble head could vary from 125 m s^{-1} to 350 m s^{-1} with an eastward velocity, in the corotating frame, of the order of 75 m s^{-1}. (In this connection we should point out that Anderson and Haerendel (1979) have shown, based on calculations performed using flux tube integrated plasma properties, that the bubble rise velocity depends significantly on the F region ambient east west electric field). Towards the end of the growth phase the rise velocity decreases significantly, whereas the eastward velocity tends to approach the eastward ambient bulk plasma drift velocity. This latter effect occurs, as explained by Tsunoda et al., (1982),due to the dependence of the bubble velocity on the bubble shape, or the axial ratio (Ossakow and Chaturvedi 1978), namely, the bubble velocity relative to the ambient plasma decreases,in direction perpendicular the bubble major axis,with increasing axial ratio. The elongated bubble at the end of the growth phase, therefore, tends to drift with ambient plasma velocities that are of the order of 100 - 200 m s^{-1}. We should note however, that these plasma bubble parameters could vary significantly from one event to another.

The meridional (namely, poleward) propagation of the airglow valleys in the N-S scanning data over Cachoeira Paulista could therefore be explained as produced either by (a) an apparent meridional component due to the eastward motion of westward tilted elongated depletion patches (or wedges), namely, the low latitude footprint of westward tilted plasma bubble, or (b) poleward propagation of the depletion corresponding to the head region as the flux tube aligned plasma bubble rises vertically upward in the equatorial ionosphere during the growth phase of an event. A third possibility is (c) the combined effects of both (a) and (b). In order to see which of these situations characterizes our results best, it is necessary to consider the different features of the valley propagation, such as,

the usual onset times of the ND's, the ratio of the valley width in the E-W to that in the N-S scan which is a measure of the westward tilt angle of the airglow patch, the typical neck to head width ratio for the plasma bubble in the equatorial plane, the E-W to N-S velocity ratio for the airglow valleys, etc.

As mentioned earlier the average local time of the first onset, in the post sunset period, of ND's considered here, is around 2100 LT which agrees within reasonable limits with the onset times of spread F in the local ionograms. We may note that the corresponding local time is ~16 minutes less at the magnetic equator where the magnetic meridian of Cachoeira Paulista intersects (due to the declination angle of 18^{o}W). The average onset time of the range type spread F usually associated with 3m backscatter irregularities, (Rastogi and Woodman, 1978), and hence with plume events) over the magnetic equatorial station, Fortaleza, is around 1900 LT, which could be assumed to precede the bubble event by about 35 minutes, (due to the oblique reception by the ionosonde), the average time difference observed at Cachoeira Paulista, mentioned earlier. If we consider also the bubble growth time, of the order of 50 minutes, (during which the vertical rise velocity is much higher than the eastward velocity as shown by Tsunoda, 1981) it is justifiable to assume that the plasma bubble development for many of the events considered here must have taken place in the immediate vicinity of the magnetic meridian of Cachoeira Paulista. The following additional points should be considered.

(a) In Figure 4 we have presented some additional events of poleward propagating valleys (unlike in the Figure 1 we do not have simultaneous east-west scan measurements for these cases). The onset of a pronounced event in part(b) of this figure can be seen at 1953 LT. The mean width of the valley (W_{NS}) calculated from 12 profiles is 670 km (note that the horizontal scale is linear in angle but not in distance). If we assume 200 km to be the eastward dimension (W_{EW}) of the bubble (Tsunoda et al., 1982) then the westward tilt (θ_t) of the airglow depletion patch, given by $\tan\theta_t \simeq W_{EW}/W_{NS}$, is $\sim 17^{o}$. The

corresponding tilt in the equatorial plane is estimated as $\sim 38^{o}$ which is reasonable (see Tsunoda, 1981). If the poleward velocity for this case, estimated to be 100 m s^{-1} as mean value determined from several valleys, is an apparent velocity (V_{SA}) caused by eastward propagation of the depletion wedges (corresponding to the neck region of a developed bubble), then the eastward velocity should be of the order of $V_E = V_{SA} \tan\theta_t \simeq 40$ m s^{-1}. This is admitedly too small compared to the bulk plasma velocity. One might, therefore, argue that the apparent poleward movement could still be caused by a bubble which is in its growth phase when the V_E is usually small. For this argument to be valid it should be necessary that V_E, and hence the apparent poleward velocity, should be increasing with time (approaching the bulk plasma velocity) as the bubble gets more and more elongated vertically. The shear flow patterns deduced by Tsunoda et al. (1981) and Kudeki et al. (1981), from backscatter radar measurements, would suggest eastward velocities over the equator of 100 - 150 m s^{-1} in the height regions relevant for the effects observed over Cachoeira Paulista. We, however, notice a reduction in the velocities toward the south (with increase in time) both in the Figure 4 as well as in the mean statistical behaviour presented in Figure 2. In fact this feature appears to be very similar to the reduction in rise velocity towards the end of the growth phase of a plume event as observed by Tsunoda (1981). Therefore, the hypothesis that the poleward velocities in these examples could be caused by the eastward propagation of the neck region of a developed bubble seems to be untenable.

(b) The estimated N-S width of the valleys in the events of the Figures 1 and 4(b) are 670 ± 52 km and 766 ± 72 km respectively, which are typical for the majority of the events considered here. The vertical dimensions in the equatorial plane for these cases would be 260 ± 20 km and 306 ± 28 km. The tilt angles of these bubbles in the equatorial plane are estimated as 51^{o} and 38^{o} (assuming W_{EW} = 200 km for the latter case) respectively. For these tilts the vertical dimensions deduced above are more likely to represent the head region rather than neck region of the bubble (see, for example, the bubble cross

section transverse to the magnetic field depicted by Tsunoda et al., (1982) and also the depletion profile measured by incoherent scatter made by Tsunoda (1981)).

(c) A very important aspect of the event in Figure 4(b) is that the onset of the valley occurs near the vertical of the station before the valley propagates southward. If the meridional propagation is an apparent effect caused by the footprint of a developed bubble drifting from the west of the meridian of Cachoeira Paulista then it should be clearly visible also in the northern portion of the scanning range. The relatively early local times of its occurrence, however, could not have permitted its generation westward of the scanning meridian. It is clear, therefore, that the bubble onset for this case occurred very close to and perhaps even slightly eastward of the meridian over Cachoeira Paulista so that a fast rise velocity and a slow eastward velocity during the growth phase of a westward tilted and vertically developing bubble (Tsunoda, 1981) might have caused the head region of the bubble, due to its finite width, to remain in the meridional scanning plane for the long duration for which this event was observed (it is worthwhile to mention here that in some recent data of simultaneous E-W and N-S scanning measurements we have observed onset of the valleys east of the meridian, which then propagated eastward and southward in the respective scanning data). A sketch of this interpretation is presented in the Appendix 2.

Also, in the case of the first event in Figure 1 it may be noted that the airglow valleys did not originate from the western (and perhaps also northern) extremities of the scanning range but from some intermediate position of the scan, and they continued to propagate till the eastern and southern limits of the scanning range. This observation seems to suggest that the bubble onset must have occurred reasonably close to the magnetic meridian of Cachoeira Paulista. Therefore the vertical rise of the bubble head and the eastward drift of the head region and/or the neck might have been responsible for the poleward and eastward displacements respectively of the airglow valleys.

A sketch of a most likely orientations of the depletion giving rise to the valley propagation for this case is also presented in the Appendix 2. In the light of the foregoing discussion it appears that we have to consider two types of events.

(1) Events for which the plasma bubble onset occurs near the magnetic meridian of the photometers which therefore detects southward propagation of the airglow valleys caused by vertically rising depleted head, having,a finite east-west dimension, covering the growth phase of an event. For this case it is possible to determine the rise velocity of the bubble in the equatorial ionosphere from the meridional velocity of the valleys.

(2) Events corresponding to post growth phase of plasma bubble that had onset at longitudes well westward of that of the photometer. In this case the photometer could detect an apparent meridional propagation of the airglow depletion produced by the eastward movement of north-south elongated and westward tilted depletion patches. (The eastward velocity for this case is that of the E-W airglow valley and can be deduced, in a straightforward way, from the meridional velocity if we know the westward tilt of the airglow patch). The second event starting at 2341 LT in Figure 4(a) could very well be an example of such an event since it is clearly visible in the northern positions of the scanning range. The first event in this figure in which the valley does not seem to originate from the northern limit of the scan could be an example of the type 1 events.

In the following we have carried out a numerical simulation of the meridional (or poleward) propagation events typical of the type (1) described above to which most of the events included in Figure 2 especially those occuring in the early post sunset hours belong to. This will be done using a two dimensional modelling based on collisional Rayleigh-Taylor instability conditions, of the depletion electron density contours in the equatorial plane, following the method of Ossakow et al. (1979). The vertical rise velocity and the vertical

depletion profile will be calculated for the average ionospheric conditions over the equator that best represented the photometer measurements. By field line projection methods these velocities will then be used to determine the expected velocities of the meridional airglow valleys. These velocities will then be compared with those determined from the meridional scan photometer in order to verify if indeed the events considered here represent the type (1) events described above.

NUMERICAL SIMULATION OF THE PLASMA BUBBLE

The [OI] 6300 Å intensity, as seen by the photometer, was calculated in the entire photometer scanning range, assuming electron density profiles perturbed by field aligned plasma density depletion. The plasma bubble that has apex at the magnetic equator was assumed to extend down to an arbitrary height of 150 km in the low latitude ionosphere. Numerical simulation of the plasma instability growth by Rayleigh-Taylor mechanism in the collisional domain was carried out, based on the formulation described by Ossakow et al. (1979). Our simulation is very similar to their ESF-3 case. For details of the simulation see the Appendix 1. The ambient electron density profile used by us in the simulation corresponds to a Chapman function with scale heigh H = 35 km below the peak and H= 45 km above the peak of the F-layer, which was taken as 430 km, in agreement with the mean hpF_2 value determined from the ionogram over Fortaleza for the period of the airglow observation. The neutral atmosphere was based on Jacchia (1977) model to represent the atmospheric conditions of March 1978 with T_∞ = 1200 K, which might approximate to the mean thermospheric conditions for our observations.

Figure 5(a) and (b) shows contour plots of constant n/n_0 at t=500 s and t=1450 s in the equatorial (east-west) plane. The contours represent only half of the bubble cross section since the other half is symmetric with the vertical y axis. The contours that have plus sign indicate enhancements and those having minus sign

represent depletions over the ambient ionization density. The broken curve represents the vertical ambient ion density distribution used for the simulation. The contours of n/n_0 obtained by us are similar to those presented by Ossakow et al. (1979) for their ESF-3 case. The vertical rise velocity of the bubble for the case presented here comes out to be 120 m s^{-1}. The electron density height profile along the bubble vertical axis of symmetry for t = 1450 s is presented in Figure 6(a). An accumulation of ionization can be observed below the depletion region, which results from the fact that the ionization that is removed from the depletion region is thrown to lower heights. However, such large ionization accumulation should not be present in the real ionosphere, since our simulation, which is in two dimensions only, may not represent the real case. Diffusion, along the field lines to lower heights, of this accumulation, followed by recombination, would cause their rapid disappearence. Ionization accumulation resulting from bubble formation has not so far been detected by radars, rockets or satellites. In determining the electron density profile disturbed by plasma bubble, for use in the airglow simulation, we have not included the part of the profile in Figure 6(a) that represents ionization accumulation. This is mainly because the field aligned depletion that rises upward over the magnetic equator, has its extremities propagating away from the equator over the low latitude where the airglow observation was carried out. On the other hand, any possible ionization accumulation, even if produced with the development of a bubble, should be descending downward over the equator (see, also, Ossakow et al., 1979), so that the field alignment of the ionization would probably confine it to the regions close to the magnetic equator.

SIMULATION OF THE NORTH-SOUTH PROPAGATING AIRGLOW VALLEYS

The calculation of the airglow intensity as a function of zenith angle, as seen by the photometer, involved the following considerations:

a) A simple Chapman function was used to represent the unperturbed electron density height profile. But the peak density and its height were assumed to vary with latitude as shown in Figure 7, to include the Appleton anomaly. This latitudinal distribution was based on the work of Lyon and Thomas (1963) and Hanson and Moffett (1966). The electron density at the F-layer peak at Cachoeira Paulista was taken to be 1.8×10^6 cm^{-3}, based on its average value during summer months at 20 LT, obtained from ionosonde.

b) The thickness of the plasma bubble, seen by the photometer, changes with zenith angle. In Figure 8 we have depicted a meridional cross section of a westward tilted, vertically elongated and flux tube aligned plasma bubble whose low latitude extremities extend to an altitude of about 150 km in the lower F-region. (It should be noted here that the bubble dimensions discussed before are not represented to the scale in this figure which serves to illustrate only the procedure used to obtain the depletion electron density profile used in the calculation of the airglow meridional profile, and that the neck of the bubble does not lie in the plane of this figure). Initially the thickness D, illustrated in Figure 8, was determined for each zenith angle, which was then projected in vertical direction as the thickness D_v. The depletion profile that has a thickness d in the equatorial plane, namely perpendicular to the magnetic field line, was then used, by interpolation, to obtain a profile having thickness D_v. The depletion profile so calculated was superposed on the background electron density profile to obtain the profile perturbed by the plasma bubble. In Figure 6b we have presented an electron density profile over the equator perturbed by a bubble at an altitude of 550 km. The corresponding perturbed profile over the low latitude, Cachoeira Paulista, obtained by projection of the same bubble is presented in Figure 6c.

c) The airglow intensity, in Rayleighs, in the direction α of the photometer looking zenith angle was integrated using the following formula (Sobral, 1973):

$$I(6300) \simeq 10^{-1} \text{ Sec } (\alpha) \int_{h_1}^{h_2} \frac{A(6300)}{A+Q[N_2]} R\gamma_1[O_2]\,[e]F\,dh \qquad (1)$$

where,

$$F = \frac{[O^+]}{[e]} = 1/(1 + (\gamma_1[O_2]/\alpha_1[e] + \gamma_2[N_2]/\alpha_2[e])),$$

[X] is the concentration of the element X, e stands for electron, A(6300) is the Einstein coefficient for emission, A = A(6300)+A(6393)+ A(6394), Q is the quenching coefficient of the excited oxygen atoms by collisions with N_2, R is the average number of atoms $O[^1D]$ produced by the dissociative recombination of O_2^+ ($O_2^+ + e \rightarrow O + O + 6.96$ eV), h is the height and α_1, γ_1, α_2, γ_2 are the reaction rate coefficients, respectively, of the following reactions:

$$O_2^+ + e \rightarrow O + O + 6.96eV,$$

$$O^+ + O_2 \rightarrow O_2^+ + O + 1.53eV,$$

$$NO^+ + e \rightarrow N + O + 2.76eV,$$

$$O^+ + N \rightarrow NO^+ + 1.09eV.$$

The constants of the equation (1) used are the same as those of Sobral (1973). Numerical integration of the equation (1) was carried out for height range 150 km to 600 km using height slabs of 4 km.

RESULTS OF THE SIMULATIONS, AND DISCUSSION

The meridional profiles of the 6300 Å nightglow intensity calculated according to the procedure described above is presented in Figure 9. The profiles presented are for different values of the apexes (h_o) of the plasma depleted tubes over the magnetic equator. We can see clearly that, as the bubble rises up over the magnetic equator, the airglow intensity valleys propagate from north to south in agreement with the experimental observations. For a bubble vertical velocity of 120 m/s, that resulted from the numerical simulation of the bubble, it takes 14 minutes for the bubble to rise from 450 km to 550 km over the magnetic equator, while at the same time airglow intensity valley propagates by approximately 270 km at a reference height of 300 km over the low latitude ionosphere. This yields a velocity of 320 m/s for the airglow disturbance on the northern side of Cachoeira Paulista. Similarly, when the bubble rises from 650 km to 750 km the airglow valley gets dislocated meridionally by approximately 240 km resulting in a velocity of 285 m/s to the south side of Cachoeira Paulista. These results are in excellent agreement with the experimental results of Table 1, that yielded the velocities to north and to south of the station to be 305 ± 159 m/s and 246 ± 150 m/s, respectively. This agreement appears to provide a strong evidence that the regions of plasma depletion associated with the airglow valleys are strongly aligned with the magnetic field. The latitudinal gradient in the background airglow intensity in Figure 8 is produced by the Appleton anomaly.

We should point out that the above results were obtained assuming height independent vertical bubble rise velocities, which may not be necessarily true in the individual cases of the vertical bubble propagation. For example, theoretical calculations by Anderson and Haerendel (1979) have shown the rise velocity increasing with altitude, in agreement with the dependence of the rise velocity on the degree of depletion during the development phase, as shown by Ossakow et al. (1979). On the other hand radar observations by Tsunoda (1981) have shown decrease in the rise velocity towards the end of the growth phase of a

plume event. These two trends in the rise velocity that characterize the successive phase of an event should be present in the statistical results in Figure 2. To what extent these effects overcome the geometrical effect of field line projection (namely, a decrease in the velocity southward for a constant vertical rise velocity over the equator) can only be determined by more detailed analysis of individual events. However, since the low latitude positions, especially the southern scanning positions, are unlikely to observe the early growth phase of a bubble, the observed decrease in the poleward velocities seen in the statistical trend in Figure 2 is more likely to represent the rise velocity decrease observed Tsunoda (1981). Such an inference seems to be favoured by the fact that the observed southward decrease in the mean velocities shown in Table 1 tend to be somewhat higher than that expected purely from the field line projection effect mentioned above.

Figure 9 further shows that the amplitude of the airglow perturbation decrease from north to south, which seems to agree with the observation (Figure 3). This effect could be due to the geometrical factor of the bubble as seen by the photometer, which would be a function of the cross sectional size of the bubble in relation to the thickness of the airglow emitting layer. Another factor that could cause this type of variation could be a possible decrease in the degree of plasma depletion at the extremities of a bubble as it extends poleward while rising over the equator. Another possibility, perhaps related to the latter point, could be that the percentage depletion caused by the bubble might, in some way, be more in regions of lower ambient density as compared to regions of higher ambient density so that the presence of the Appleton anomaly crest on the southern side of the observing site, which seems to be generally the case at these hours, might be responsible for the similar trends in the observed and calculated airglow disturbance amplitudes.

In the foregoing discussion we have assumed that plasma bubbles develop vertically upward and tilted westward in the equatorial

ionosphere, and the simultaneous development of a bubble along a flux tube causes vertical rise velocity of the bubble translated into the poleward motion that is detected by the meridional scanning photometers over the low latitude. Therefore, the duration for wich a bubble remains in the meridional scanning plane would depend upon the bubble shape, tilt angle and velocity in the equatorial plane. In fact, it is the combination of the east-west dimension, the westward tilt angle and the eastward to vertical velocity ratio that would determine the duration for which a given airglow valley would be observed by the meridional scan photometer. It is possible to come across frequent situations in which the bubble head would remain in the immediate vicinity of the meridional plane while the foot of the bubble would be displaced eastward with progress of time somewhat similar to the situation depicted in the Appendix 2.

CONCLUSIONS

Airglow disturbances observed by east-west and north--south scanning photometers over the low latitude station, Cachoeira Paulista are manifestations of the equatorial plasma bubble dynamics. The individual and statistical characteristics of a number of events are analysed in this paper in an attempt to infer important parameters of the plasma bubble dynamics. While the interpretation, that the eastward propagating airglow valleys observed in the east-west scan photometer represent a corresponding eastward propagation of the equatorial plasma depletion, is rather straightforward, that of the poleward propagation of the airglow valleys observed in the north-south scan photometer involves careful considerations on the phase of a bubble event. Information on the plume and plasma depletions obtained from the ALTAIR streerable radar (Tsunoda et al., 1981; Tsunoda 1980, 1981) and the 6300 Å images taken over low latitudes (Weber et al. 1980, Mendillo, 1982) have greatly helped the interpretation of our scanning data. Two types of the plasma depletion effects on the meridional scan data have been considered. One of them is caused by the plasma bubble events that have onset well westward of the longitude of the observation

so that the footprint representing the post development phase of these events (namely, north-south elongated depletion wedges moving eastward) will cause eastward propagation of airglow valleys in the east-west scanning photometer while at the same time causing an apparent poleward propagation of the valleys in the north-south scanning photometer. Once an event is identified as belonging to this phase the interpretation of the airglow valleys is rather straightforward. The other type of event represents the onset of the plasma bubble in the immediate vicinity of the magnetic meridian of the photometer (and hence the growth phase of an event) in which case, therefore, the north-south scan photometer detects poleward propagation of the airglow valleys caused by vertically rising depleted head region having finite east--west dimension. All the ND events observed in the early hours of the post sunset period could be considered to be belonging to this type of event (while the events detected at later hours may or may not belong to this type). We have concentrated our attention to this type of events by carrying out detailed numerical simulation of the same. This involved two dimensional numerical modelling of the plasma bubble, generated under the collisional R-T instability conditions, to determine the equatorial rise velocity and the ion density depletion profiles under the average ionospheric conditions of the observations, that were then used to simulate the meridional propagation of the airglow valleys. The excellent agreement obtained between these results and those observed from our meridional scanning measurements supports our contention that those cases do indeed represent the airglow manifestation of the vertical rise velocity of the head region of a plasma bubble in its growth phase. The statistical behaviour in the observed mean meridional velocity, namely, a poleward decrease, as observed also in many individual cases, seems, in fact, to support the radar results (Tsunoda, 1981) of the plasma bubble rise velocity decrease observed towards the end of the growth phase of a plume event. The latitudinal variation in the mean amplitude of the airglow valleys observed from the north-south scan measurement also agrees with the results obtained from the numerical simulation. The results from the present analysis, therefore, show that depending upon the identification

of an ND as representing the growth phase or the post growth phase of a plasma bubble event, we can deduce interesting parameters of the equatorial plasma bubble dynamics from such data. Further analysis is continuing using more recent data available from these measurements.

ACKNOWLEDGEMENTS

This work was partially supported by the "Fundo Nacional de Desenvolvimento Científico e Tecnológico" under contract FINEP-130/CT.

Appendix 1

Consideration Involved in the Numerical Simulation of Plasma Bubble by R - T Mechanism under Collisional Regime

Briefly, our numerical simulation has the following features. Ossakow et al., (1979) have derived equations appropriate for numerical integration starting from the basic plasma two-fluid equation describing the system, namely:

$$\partial n/\partial t + \nabla.(n_\alpha \bar{V}_\alpha) = \nu_R(n_\alpha - n_{\alpha 0}) \quad (1)$$

$$(\partial/\partial t + \bar{V}_\alpha \cdot \nabla)\bar{V}_\alpha = (q_\alpha/m_\alpha)\left(\bar{E} + \frac{\bar{V}\times\bar{B}}{c}\right) + g - \nu_\alpha \bar{V}_\alpha \quad (2)$$

where the subscript α denotes the species (i for ions and e for electrons), n is the species number density, $\bar{V}$ is the velocity, ν_R is the recombination coefficient, $\bar{E}$ is the electric field, $\bar{g}$ is the gravitational acceleration, q is the species charge, ν_R is the collision frequency of the species with neutral particles, c is the speed of light and m is the species mass.

The geometry of the equatorial spread F and all the assumptions of approximations made are the same as those of Ossakow et al.,(1979). Therefore, we carried out numerical integration of the equations (23) and (24) of Ossakow et al., (1979) that describe the potential and the electron density distribution with time in the equatorial plane. The mesh size of the integration used was 2 km in the vertical y direction and 200 m in the eastward x direction, and the simulation was performed over an altitude interval of 200 km within an east-west extension of 8 km. Equation (23) was integrated forward in time using flux-corrected transport algorithms (Boris and Book, 1973) while equation (24) was solved using successive over--relaxation (SOR) method. Periodic boundary conditions were imposed on both n and ϕ_1 (the perturbed electrostatic potential) in the x

direction. In the y direction, transmissive boundary conditions were imposed on n, ($\partial n/\partial y = 0$), and Neumann boundary condition ($\partial \phi_1/\partial y = 0$) was imposed on ϕ_1. The initial perturbation superimposed on the background density over the entire mesh was the same as that of Ossakow et al. Our simulation was performed for conditions similar to those representing the ESF-3 case of Ossakow et al.

Appendix 2

Sketches of the low latitude footprint of plasma bubbles represented by the airglow scanning data of Figures 1 and 4 in the text.

The low latitude footprint of the plasma bubbles whose signatures could have been the ones registered by the N-S and E-W scan photometer data of the Figure 1 and by the N-S scan data of the Figure 4 of the text, are sketched in the parts (a) and (b), respectively, of the Figure A1. In drawing these sketches we have considered two dimensional bubble shape, transverse to the magnetic field, as depleted wedges of ionization extending from the bottomside F-layer and having well defined "head" and "neck" regions as depicted by Tsunoda et al., (1982) based on the ALTAIR radar and AE-E satellite measurements. It should be noted that the vertical dimension in the equatorial plane will be magnified by a factor of ~2.5 while projecting along the field lines (due to the field line geometry) onto horizontal planes in the low latitude ionosphere where the scanning photometers are situated (indicated in the figure). The E-W dimension of the bubble, on the other hand, is projected down without any change. Therefore, the bubble footprint appears significantly more elongated than those sketched by Tsunoda et al. (1982) which applies for the equatorial plane.

In preparing the sketches in the part (a) we have used average valley widths both in the N-S and E-W directions as determined using most of the scanning profiles taken during the passage of the valleys, the mean widths being 766 ± 72 km and 316 ± 52 km respectively in the N-S and E-W directions. The bubble footprints are cut across by the N-S and E-W scanning planes such that the depletion widths and positions at the times marked in Figure A1 (on each of the bubble footprints) correspond to the airglow valley widths and positions in the scanning profiles identified with the same local times in the Figure 1. Only three positions of the bubble footprints are considered, for the sake of clarity of the figure, representing the beginning, the middle and the end of each event.

For the case of the sketch in part (b) of the figure the valley width in the N-S plane was monotonically decreasing toward south, and therefore we have considered three different widths (namely 814 km, 649 km and 587 km) at the three times. Since we did not have E-W scan measurements for this day approximate widths in the E-W direction have been used that were required to give a proportional shape to the bubble footprint taking into account also the airglow depletion patches photographed by Weber et al. (1980).

It may be pointed out that it is quite possible to produce sketches showing slightly different shapes for the bubble footprints using the same input informations on the valley widths versus time and positions (and possibly for different E-W widths in the case of the sketch in part (b)).Nevertheless,the sketches presented in this figure do seem to represent reasonably well the growth phase of a bubble event during which the poleward valley propagation in the scanning data can be seen as a direct consequence of the vertical growth of the westward tilted wedge shaped plasma depletions in the equatorial ionosphere (explained in more detail in the text).

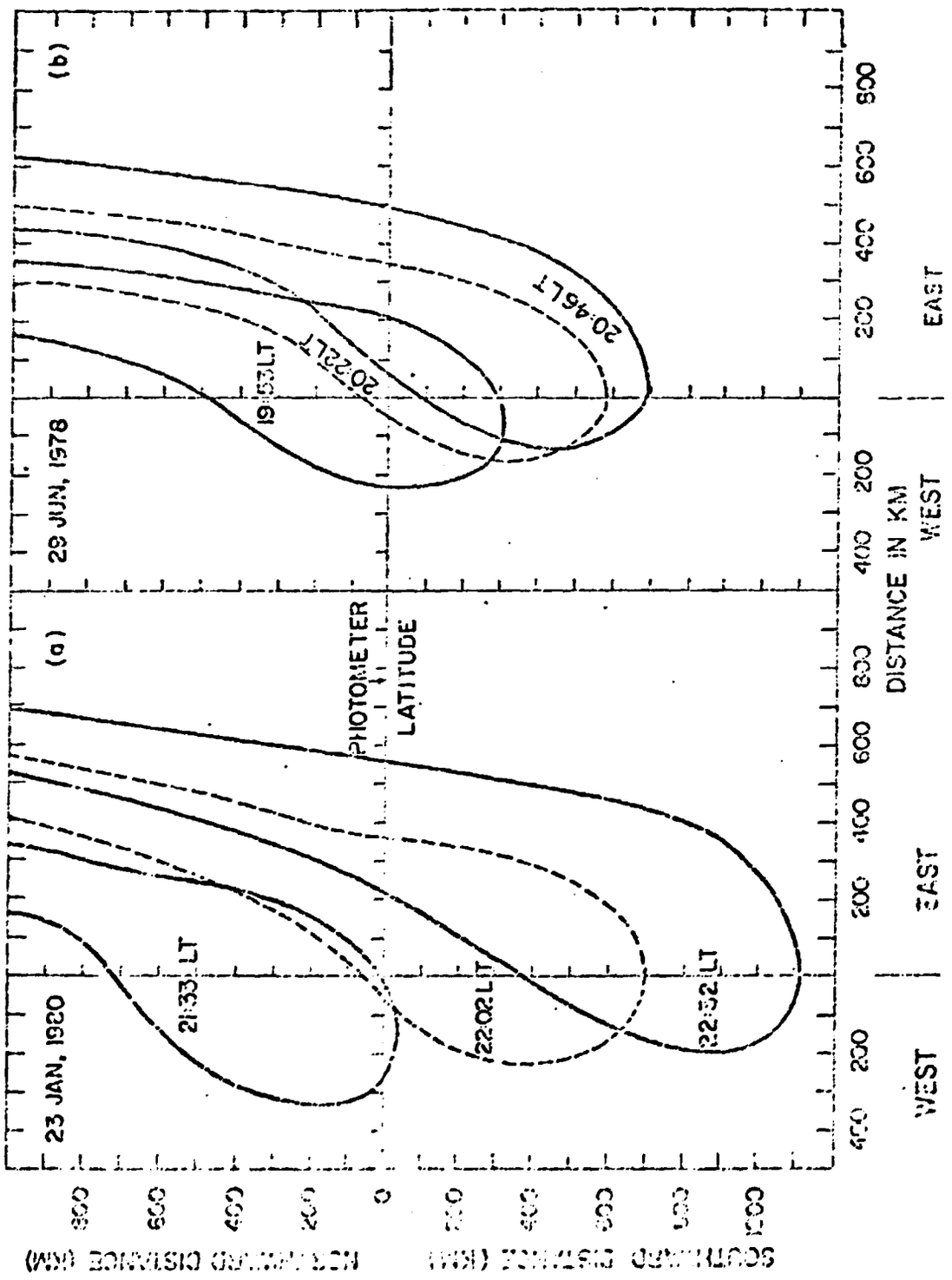
(b)
29 JUN, 1978
19:53LT
20:22LT
20:46LT
(a)
23 JAN, 1920
21:33 LT
22:02 LT
22:52 LT
PHOTOMETER
LATITUDE
DISTANCE IN KM
WEST
EAST
WEST
EAST
SOUTHWARD DISTANCE (KM)
NORTHWARD DISTANCE (KM)

Fig. A1

REFERENCES

Aarons J., Mullen J.P., Whitney H.E., Mackenzie E.M., 1980. The dynamics of equatorial irregularity patch formation, motion and decay, J. Geophys. Res., 85, 139-149.

Abdu M.A., De Medeiros R.T., Sobral J.H.A., 1982. Equatorial spread F instability conditions as determined from ionograms, Geophys. Res. Lett., 9, 692-695.

Anderson D.N., Haerendel G., 1979. The motion of depleted plasma regions in the equatorial ionosphere, J. Geophys Res., 84, 4251-4256.

Basu S., Kelley M.C., 1979. A review of recent observations of equatorial scintillations and their relationship to current theories of F region irregularity generation, Radio Sci., 14, 471-485.

Boris J.P., Book D.L., 1973. Flux-corrected transport, I, Shasta, a transport algorithm that works, J. Comput. Phys., 11, 38-69.

Chaturvedi P.K., Kaw P.K., 1975. Steady state finite amplitude Rayleigh-Taylor mode in spread-F, Geophys. Res. Lett., 2, 499.

Dachev Ts. P., Walker J.C.G., 1982. Seasonal dependence of the distribution of large-scale plasma depletions in the low-latitude F Region, J. Geophys. Res., 87, 7625-7639.

Dungey J.W., 1956. Convective diffusion in the equatorial spread F region, J. Atmos. Terr. Phys., 9, 304-310.

Dyson P.L., Benson R.F., 1978. Topside sounder observations of equatorial bubbles, Geophys. Res. Lett., 5, 795-798.

Haerendel G., 1973. Theory of equatorial spread F, Preprint., Max-Planck Institut, Garching, West Germany.

Hanson W.B., Moffet R.J., 1966. Ionization transport effects in the equatorial F region, J. Geophys. Res., 71, 5559-5572.

Hanson W.V., Sanatani S., 1971. Relationship between Fe^+ ions and equatorial spread F, J. Geophys. Res., 76, 7761-7768.

Hudson M.K., Kennel C.F., 1975. Linear theory of equatorial spread-F, J. Geophys. Res., 80, 4581-4590.

Jacchia L.G., 1977. Thermospheric temperature, density and composition: new models, Smithson. Astrophys., Special Report 375.

Kelley M.C., Haerendel G., Koppler H., Valenzuela A., Balsley B.B., Carter D.A., Ecklund W.L., Carlson C.W., Hansler B., Torbert R., 1976. Evidence for a Rayleigh-Taylor type instability and upwelling of depleted density regions during equatorial spread F, Geophys. Res. Lett., 3, 448-450.

Kudeki E., Fejer B.G., Farley D.T., Ierkic H.M., 1981. Interferometer studies of equatorial F-region irregularities and drifts, Geophys. Res. Lett., 8, 377-380.

Lyon A.J., Thomas L., 1963. The F2-region equatorial anomaly in the African, American and East Asian sectors sunspost maximum, J. Atmos. Terr. Phys., 25, 373-386.

McClure J.P., Hanson W.B., Hoffman J.F., 1977. Plasma bubbles and irregularities in the equatorial ionosphere, J. Geophys. Res., 82, 2650-2656.

Mendillo M., Baumgardner J., 1982. Airglow characteristics of equatorial plasma depletions, J. Geophys. Res., 87, 7641-7652.

Moore J.G., Weber E.J., 1981. OI 6300 and 7774 Å airglow measurements of equatorial plasma depletions, J. Atmos. Terr. Phys., 43, 851-858.

Morse F.A., Edgar B.C., Koons H.C., Rice C.J., Heikkila W.J., Hoffman J.H., Tinsley B.A., Winningham J.D., Christensen A.B., Woodman R.F., Pomalaza J., Teixeira N.R., 1977. Equion, an equatorial ionospheric irregularity experiment, J. Geophys. Res., 82, 578-592.

Ossakow S.L., Zalesak S.T., McDonald B.E., Chaturvedi P.K., 1979. Nonlinear equatorial spread F: Dependence on altitude of F peak and bottomside background electron density gradient scale length, J. Geophys. Res., 84, 17-29.

Ott E., 1978. Theory of Rayleigh-Taylor bubbles in the equatorial ionosphere, J. Geophys. Res., 83, 2066-2070.

Reid G.C., 1968. The formation of small scale irregularities in the ionosphere, J. Geophys. Res., 73, 1627-1640.

Rishbeth H., 1971. Polarization fields produced by winds in the equatorial F-region, Planet. Space Sci., 19, 357-369.

Sahai Y., Bittencourt J.A., Teixeira N.R., Takahashi H., 1981. Plasma irregularities in the tropical F-region detected by OI 7774 Å and 6300 Å nightglow measurements, J. Geophys. Res., 86, 3496-3500.

Scannapieco A.J., Ossakow S.L., Goldman S.R., Pierre J.M., 1976. Plasma cloud late time striation spectra, J. Geophys. Res., 81, 6037-6045.

Sobral J.H.A., 1973. Airglow and incoherent scatter studies of the dynamics of the nighttime ionosphere at Arecibo, PhD. dissertation, Cornell University, Ithaca, New York, 1973.

Sobral J.H.A., Abdu M.A., Batista I.S., 1980a. Airglow studies on the ionosphere dynamics over low latitude in Brazil, Ann. Geophys., 36, 199-204.

Sobral J.H.A., Abdu M.A., Zamlutti C.J., Batista I.S., 1980b. Association between plasma bubble irregularities and airglow disturbances over Brazilian low latitude, Geophys. Res. Lett., 7, 980-982.

Sobral J.H.A., Abdu M.A., Batista I.S., Zamlutti C.J., 1981. Wave disturbance in the low latitude ionosphere and equatorial ionospheric plasma depletions, J. Geophys. Res., 86, 1374-1378.

Tsunoda R.T., 1980. Magnetic field-aligned characteristics of plasma bubbles, in the nighttime equatorial ionosphere, J. Atmos. Terr. Phys., 42, 743-752.

Tsunoda R.T., 1981. Time evolution and dynamics of equatorial backscatter plumes, 1. Growth phase, J. Geophys. Res., 86, 139-149.

Tsunoda R.T., Livingston R.C., Rino C.L., 1981. Evidence of a velocity shear in bulk plasma motion associated with the post-sunset rise of the equatorial F-layer, Geophys. Res. Lett., 8, 807-810.

Tsunoda R.T., Livingston R.C., McClure J.P., Hanson W.B., 1982. Equatorial plasma bubbles: vertically-elongated wedges from the bottomside F-layer, J. Geophys. Res., 87, 9171-9180.

Weber E.J., Buchau J., Moore J.G., 1980. Airborne studies of equatorial F layer ionospheric irregularities, J. Geophys. Res., 85, 4631-4641.

Weber E.J., Buchau J., Earther R.H., Mende S.B., 1978. North-South aligned equatorial airglow depletion, J. Geophys. Res., 83, 712-716.

Weber E.J., Brinton H.C., Buchau J., Moore J.G., 1982. Coordinated airborne and satellite measurements of equatorial plasma depletions, J. Geophys. Res., 87, 10503-10513.

Woodman R.F., La Hoz C., 1976. Radar observations of F-region equatorial irregularities, J. Geophys. Res., 81, 5447-5466.

FIGURE CAPTIONS

Fig. 1. Profiles of [OI] 6300 Å nightglow in N-S (a) and E-W (b) scanning. Each profile has the base line (intensity of [OI] 6300 Å equal to zero) identified by the local time marked also on the respective profiles. The calibration of intensity in Rayleighs is indicated at the bottom of (a).

Fig. 2. A statistical analysis of a number of events showing the positions of the airglow valleys in the meridional scan as a function of time, plotted to the north and to the south of the vertical of the point of observation. Time equal to zero is attributed to the position of the valleys at the zenith.

Fig. 3. Statistical analysis of amplitude variation of the disturbance in function of zenith angle. The straight line is the least square fit of the points. The standard deviation

$$\sigma = \left[\frac{1}{n-1} \sum_{i=1}^{N} (I_i - I_o)^2 \right]$$

was calculated for each night and for each zenith angle with 15^o of interval. For a given zenith angle, I_i is the airglow intensity at time i and I_o its mean value, for each zenith angle over n meridional profiles of airglow.

Fig. 4. Examples N-S scan airglow data showing propagating airglow valleys (a) on both the northern and southern halves, (in the earlier event), and mainly on the northern half, (in the later event), of the photometer scanning range, and (b) mainly on the southern half of the photometer scanning range starting in the early hours of the post sunset period. (see the text for further details).

Fig. 5. Ion density contours, normalized to the ambient values, perpendicular to the magnetic field and in the equatorial plane, obtained from the numerical simulation of the plasma bubble, based on the R-T mechanism under collisional regime, following the method of Ossakow et al., (1979), shown for t = 500 s (a) and t= 1450 s (b) after the onset of an initial perturbation in the ionization.

Fig. 6. (a) Ion density profiles normalized to the ambient density along the vertical axis of symmetry of the bubble, at t=500 s and 1450 s. (b) A perturbed ion density profile obtained by superposition of the quiet ion density profile with the depletion profile through the vertical bubble axis, maximum depletion being located at a height of 550 km over the equator. (c) The perturbed profile over low latitude obtained from magnetic field line projection of the equatorial profile of (b).

Fig. 7. Electron density at F layer peak (N_m) and its height (h_m) in function of magnetic latitude.

Fig. 8. Meridional cross section of an idealised field aligned plasma bubble to illustrate the procedure used to calculated the [OI] 6300 Å intensities for various zenith angles (α). h_o indicates the height of the bubble over equator and $n_o(y)$ is the electron density profile. Please note that the diagram is not to the scale.

Fig. 9. [OI] 6300 Å airglow intensity as a function of zenith angles, for different heights of the bubble (h_o) over the magnetic equator, that resulted from the numerical simulation.

TABLE 1

Velocity to the north (V_n) and to the south (V_s) of Cachoeira Paulista

Nº	V_n (m/sec)	V_s (m/sec)
1	368	339
2	388	250
3	174	501
4	379	222
5	177	121
6	271	278
7	336	142
8	443	187
9	606	244
10	180	245
11	31	180
MEAN VELOCITY	305 (σ = ± 159)	246 (σ = ± 105)

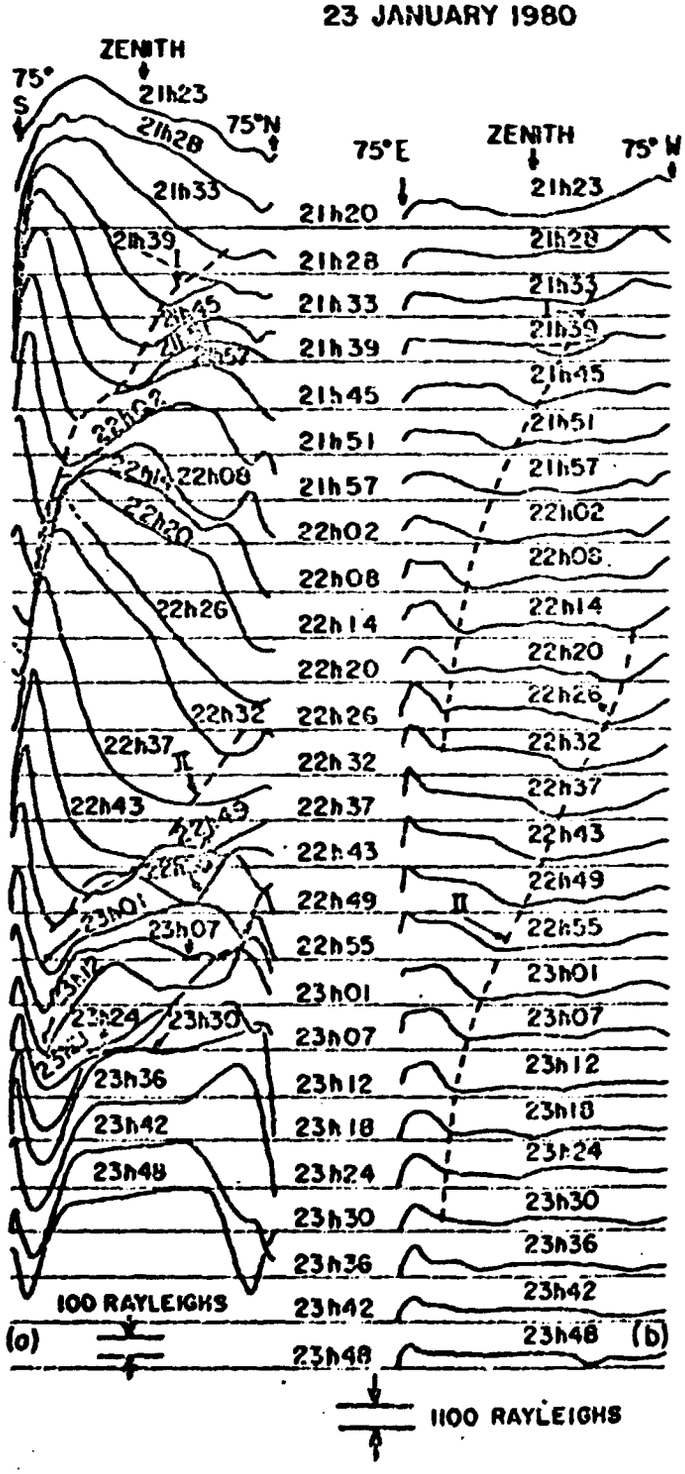
23 JANUARY 1980
ZENITH
75° S
75°N
75°E
ZENITH
75° W
100 RAYLEIGHS
(a)
(b)
1100 RAYLEIGHS

Fig. 1

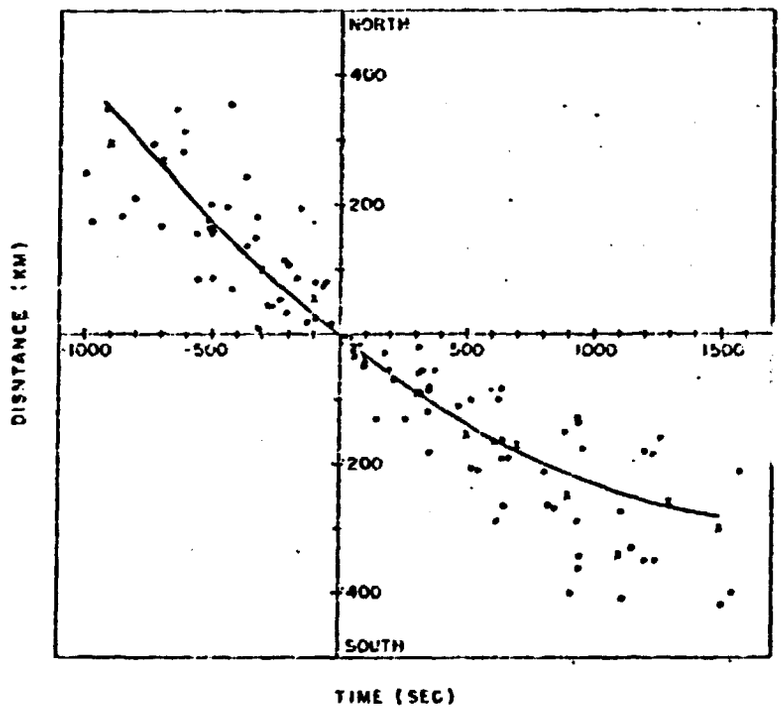
NORTH
400
200
-1000
-500
500
1000
1500
200
400
SOUTH
DISTANCE (KM)
TIME (SEC)

Fig. 2

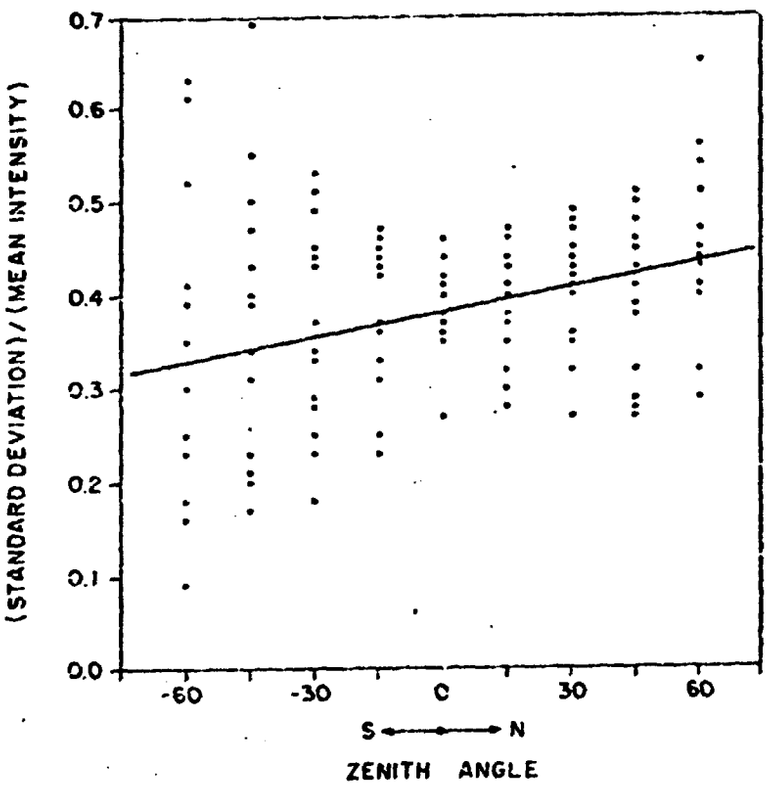
(STANDARD DEVIATION) / (MEAN INTENSITY)
0.7
0.6
0.5
0.4
0.3
0.2
0.1
0.0
-60
-30
0
30
60
S
N
ZENITH ANGLE

Fig. 3

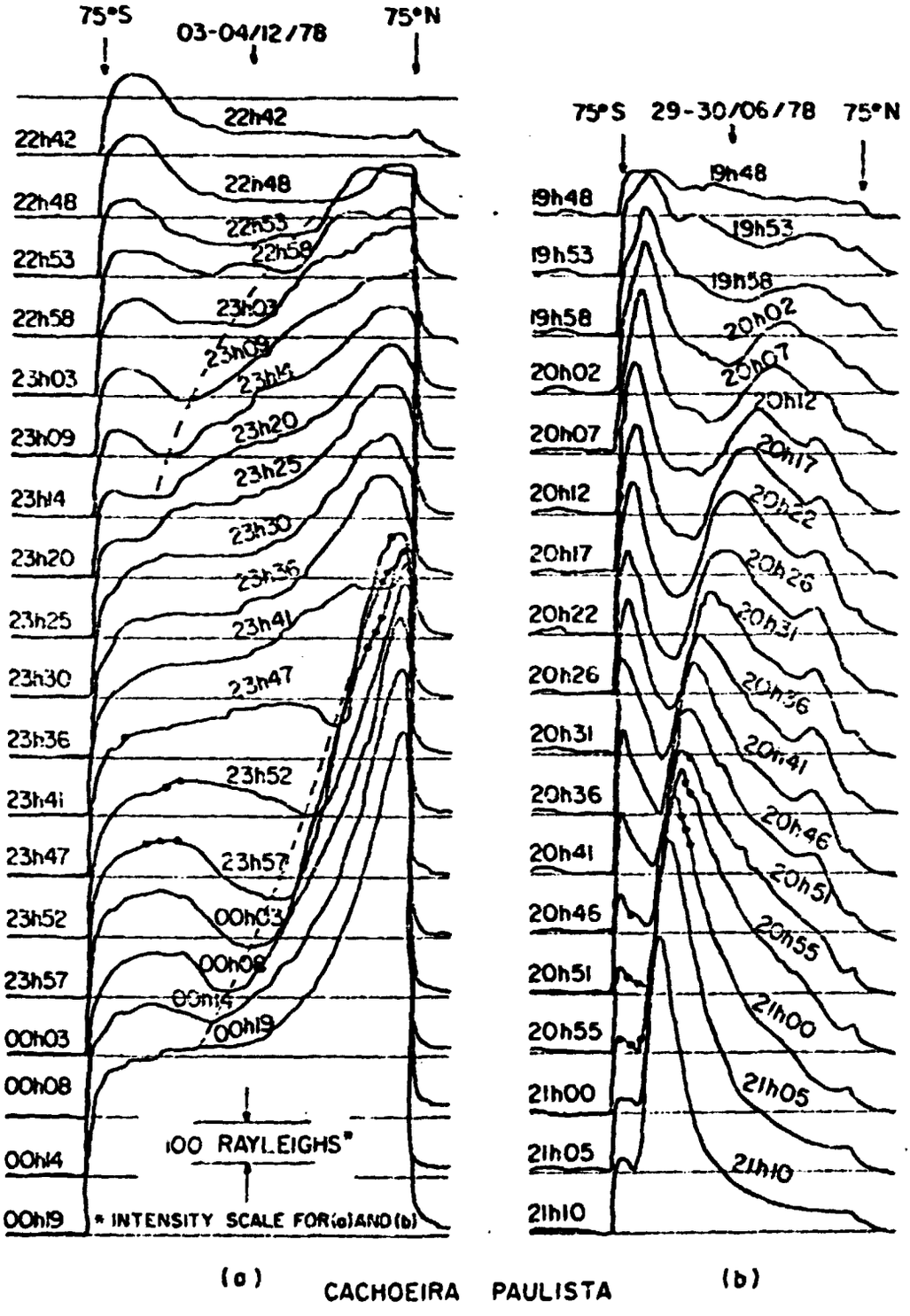
75°S
03-04/12/78
75°N
22h42
22h48
22h53
22h58
23h03
23h09
23h14
23h20
23h25
23h30
23h36
23h41
23h47
23h52
23h57
00h03
00h08
00h14
00h19
100 RAYLEIGHS*
* INTENSITY SCALE FOR (a) AND (b)
(a)
75°S
29-30/06/78
75°N
19h48
19h53
19h58
20h02
20h07
20h12
20h17
20h22
20h26
20h31
20h36
20h41
20h46
20h51
20h55
21h00
21h05
21h10
(b)
CACHOEIRA PAULISTA

Fig. 4

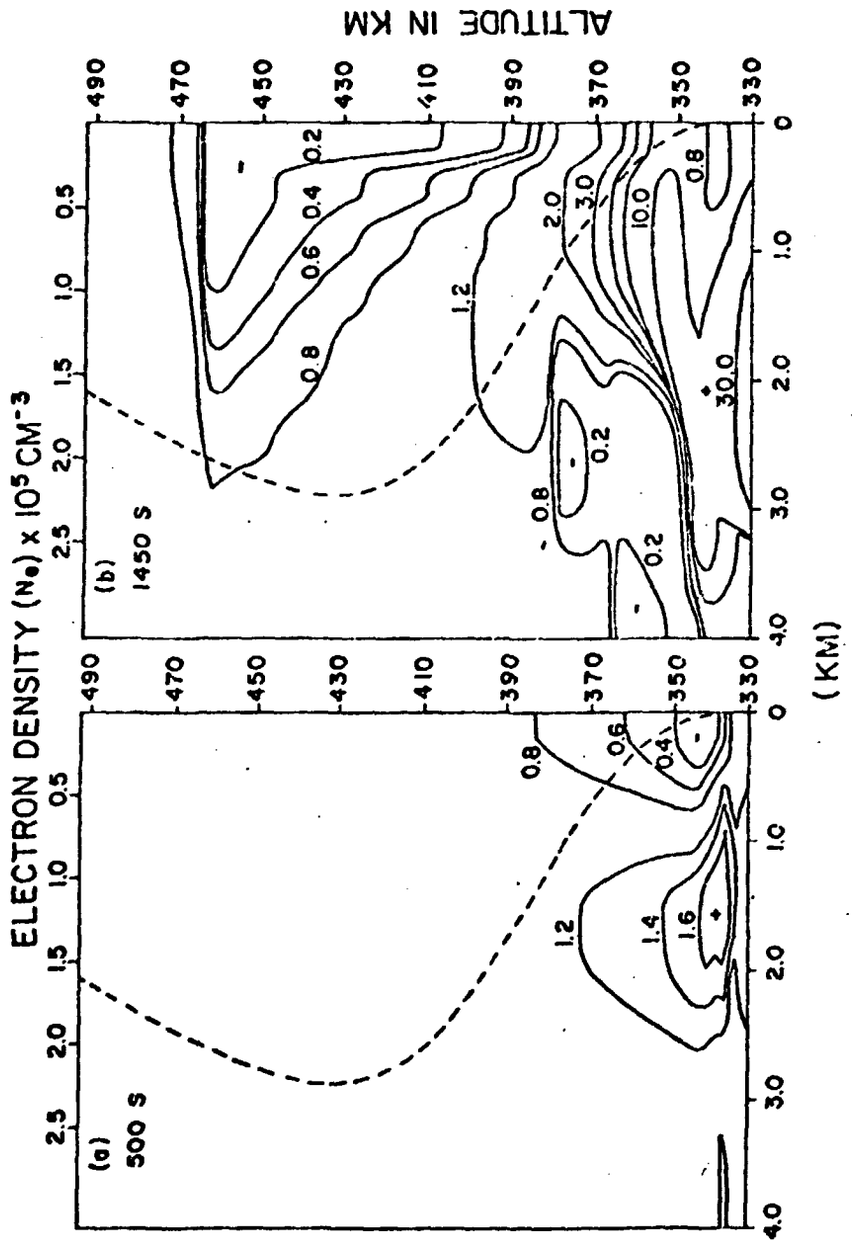

Fig. 5

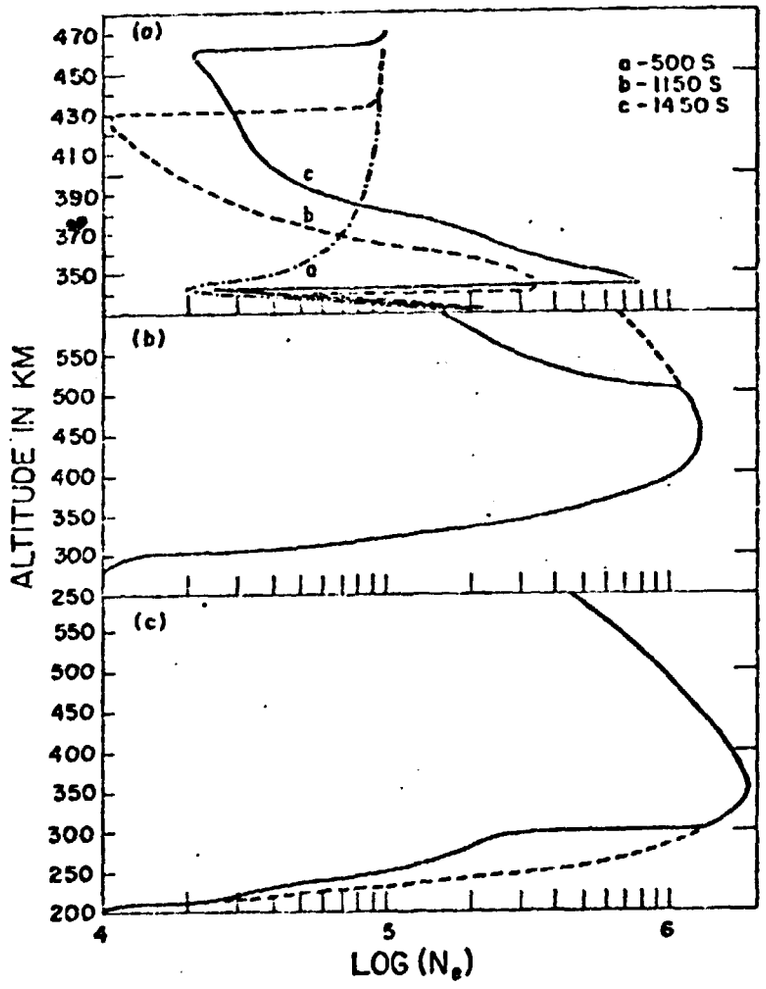
(a)
(b)
(c)
a - 500 S
b - 1150 S
c - 1450 S
ALTITUDE IN KM
LOG (N_e)
470
450
430
410
390
370
350
550
500
450
400
350
300
250
200
4
5
6

Fig. 6

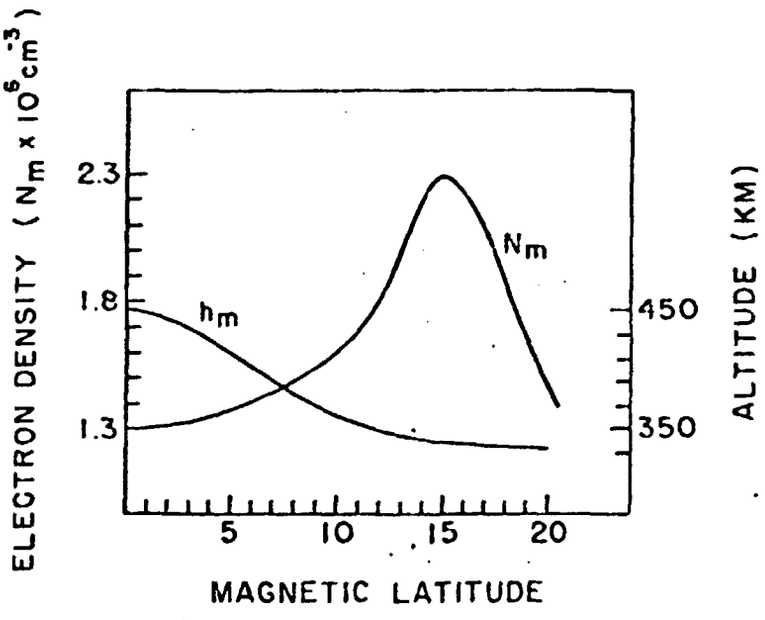
ELECTRON DENSITY ($N_m \times 10^6 cm^{-3}$)
2.3
1.8
1.3
h_m
N_m
450
350
ALTITUDE (KM)
5
10
15
20
MAGNETIC LATITUDE

Fig. 7

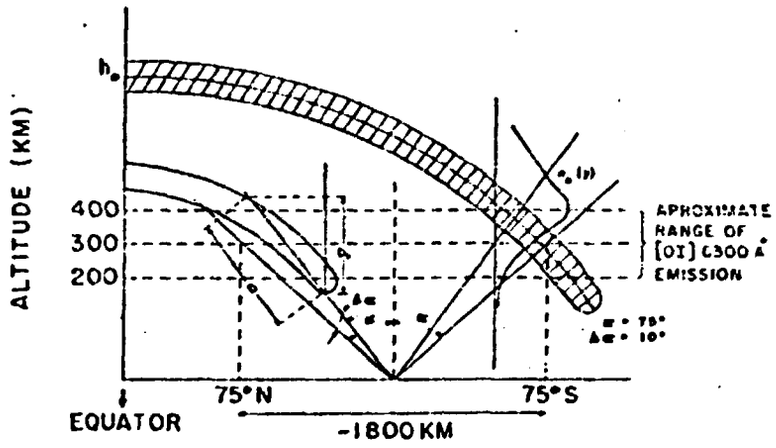
ALTITUDE (KM)
400
300
200
APPROXIMATE RANGE OF [OI] 6300 Å EMISSION
75°N
75°S
EQUATOR
~1800 KM

Fig. 8

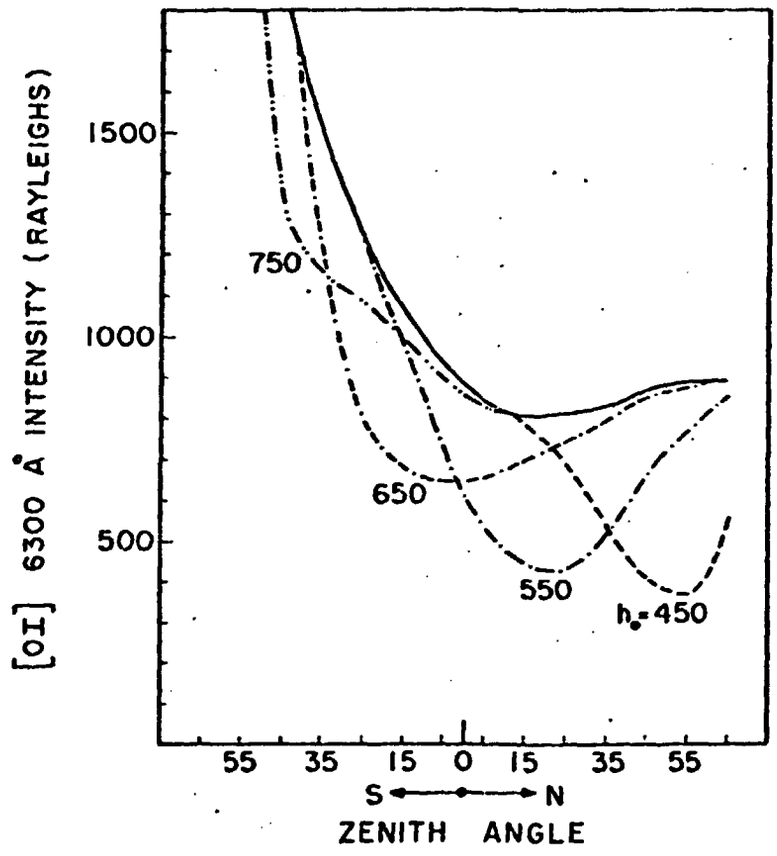
[OI] 6300 Å INTENSITY (RAYLEIGHS)
1500
1000
500
750
650
550
h₀=450
55 35 15 0 15 35 55
S ← → N
ZENITH ANGLE

Fig. 9